Lymphoma angiogenesis is orchestrated by noncanonical signaling pathways

Marleen Gloger[1,8], Lutz Menzel[1,8], Michael Grau[2], Anne-Clemence Vion[3], Ioannis Anagnostopoulos[4], Myroslav Zapukhlyak[2], Kerstin Gerlach[1], Thomas Kammertöns[5], Thomas Hehlgans[6], Maria Zschummel[7], Georg Lenz[2], Holger Gerhardt[3], Uta E. Höpken[7*], Armin Rehm[1*]

[1] Translational Tumorimmunology, Max-Delbrück Center for Molecular Medicine; 13125 Berlin, Germany
[2] Department of Medicine A, and Cluster of Excellence EXC 1003; University Hospital Münster; 48149 Münster, Germany
[3] Integrative Vascular Biology Lab, Max-Delbrück Center for Molecular Medicine; 13125 Berlin, Germany
[4] Institute of Pathology, Charité-University Medicine Berlin; 10117 Berlin, Germany
[5] Institute of Immunology, Charité -University Medicine Berlin; 13125 Berlin, Germany
[6] Regensburg Center for Interventional Immunology, University Hospital Regensburg; 93053 Regensburg, Germany
[7] Microenvironmental Regulation in Autoimmunity and Cancer, Max-Delbrück Center for Molecular Medicine; 13125 Berlin, Germany

[8] These authors contributed equally

Running title: Lymphoma angiogenesis uses noncanonical angiocrine pathways

Keywords: B-cell lymphoma, angiogenesis, transcriptome, angiocrine signaling, high-resolution imaging

*Corresponding Authors: Armin Rehm, Max-Delbrück-Center for Molecular Medicine, MDC, 13125 Berlin, Germany. Phone:49-30-94063817; Email: arehm@mdc-berlin.de (Lead Contact)
Uta E. Höpken, Max-Delbrück-Center for Molecular Medicine, MDC, 13125 Berlin, Germany. Phone: 49-30-94063330; Email: uhoepken@mdc-berlin.de

Disclosure of Potential Conflicts of Interest
The authors declare no potential conflicts of interest.

1

Abstract

Tumor-induced remodeling of the microenvironment relies on the formation of blood vessels, which go beyond the regulation of metabolism, shaping a maladapted survival niche for tumor cells. In high-grade B-cell lymphoma, angiogenesis correlates with poor prognosis, but attempts to target established pro-angiogenic pathways within the vascular niche have been inefficient.

Here, we analyzed *Myc*-driven B-cell lymphoma-induced angiogenesis in mice. A few lymphoma cells were sufficient to activate the angiogenic switch in lymph nodes. A unique morphology of dense microvessels emerged without obvious tip cell guidance and reliant on blood endothelial cell (BEC) proliferation. The transcriptional response of BECs was inflammation-independent. Conventional HIF-1α or Notch signaling routes prevalent in solid tumors were not activated. Instead, a nonconventional hypersprouting morphology was orchestrated by lymphoma-provided vascular endothelial growth factor (VEGF)-C and lymphotoxin (LT). Interference with VEGF receptor-3 and LTβ receptor signaling pathways abrogated lymphoma angiogenesis, thus revealing targets to block lymphomagenesis.

Significance

In lymphoma, transcriptomes and morphogenic patterns of the vasculature are distinct from processes in inflammation and solid tumors. Instead, LTβR and VEGFR-3 signaling gain leading roles and are targets for lymphomagenesis blockade.

Introduction

The concept of reciprocal crosstalk between malignant B cells and their microenvironment in secondary lymphoid organs (SLOs) is supported by genetic signatures found in high-grade B-cell non-Hodgkin's lymphoma (B-NHL). Gene expression profiling (GEP) of primary diffuse large B-cell lymphoma (DLBCL) samples showed that differences in the microenvironment affect patient survival after chemotherapy treatment. The stromal-1 signature, related to extracellular matrix (ECM) deposition and histiocytic infiltration, is associated with favorable outcome, whereas the angiogenesis-related signature (stromal-2 signature) is prognostically unfavorable (1). The microanatomical correlate of this angiogenesis-related signature is an increased microvessel density (MVD) (2, 3).

An essential structural and functional component of the lymphoma stroma consists of the blood and lymphatic vasculature, which besides servicing the local cells, shapes the tumor-survival niche. Anti-angiogenic strategies are based on the activities of vascular endothelial growth factor (VEGF)-family molecules in cancer-associated angiogenesis (4, 5). Lymphoma cells themselves exhibit pro-angiogenic activity as they release VEGFs, but attempts to combine multimodal chemo-/immunotherapies with VEGF inhibitors have not been beneficial in B-cell lymphoma (6, 7). Therefore, it is plausible that other non-VEGF angiogenic pathways prevail and cause enhanced vascular assembly. Lymph nodes (LNs) are equipped with specialized endothelial cell (EC) subsets that line the blood and lymphatic vasculature. A comparison of transcriptomes of fibroblastic reticular cells (FRCs), blood ECs (BECs), and lymphatic ECs (LECs) taken from naive LNs and LNs exposed to an inflammatory milieu showed marked immune cell recruitment in the

3

latter (8). However, it remains unclear whether exposure to lymphoma has the same impact on stromal cells as inflammation.

Earlier studies analyzing lymphoma-engendered alterations in ECs relied on syngeneic or xenogeneic lymphoma cells transplanted subcutaneously. In these models, marked adaptations of the lymphatic vasculature occurred, which correlated with the increased availability of VEGF-C from tumor-associated macrophages (9). However, introducing cells subcutaneously or into xenogeneic hosts does not necessarily reflect the dissemination behavior of aggressive B-cell lymphoma (10). Intravenously administered *Myc*-driven B-cell lymphoma cells enter distinctive microanatomic compartments of LN and spleen via CCR7- and CD62L-regulated mechanisms, indicating that tumor cell immigration is mediated via high endothelial venules (HEVs) (11). HEVs are segments of postcapillary venules and are characterized by specialized BECs that express chemokines and adhesion molecules required for extravasation of lymphocytes into LN parenchyma (12). Within the niche, lymphoma cells stimulate reciprocal crosstalk with $CD45^-/gp38^+$ FRCs in a lymphotoxin β receptor (LTβR)-dependent manner (13). During an immune response, activated lymphotoxin α (LT) expressing B-cells directly induce differentiation of ECs into a HEV phenotype (14, 15). The precise contribution of morphogenic cells and molecular factors to angiogenesis is likely to vary depending on the stimuli, and it remains unclear whether lymphoma B-cell exposure engenders a condition that phenocopies high MVD. Here, we explored lymphoma-induced LN vascular reprogramming in an Eμ-*Myc* lymphoma-transplanted mouse model. GEP of FRCs, LECs, and BECs and comparison of angiogenic factors expressed by stroma and

lymphoma cells revealed that mechanisms different from conventional solid tumor

angiogenesis are active in B-cell lymphoma-exposed LNs.

5

Materials and Methods

Mice

The full list of mice used is given in Supplementary Materials and Methods. All experiments were conducted in compliance with the institutional guidelines of the Max-Delbrück-Center for Molecular Medicine, Berlin, Germany and approved by the Landesamt für Gesundheit und Soziales Berlin, Germany (G0104/16; G0052/12; G0373/13; G 0058/19).

Human tissue specimens and immunohistochemistry

Formalin-fixed paraffin-embedded biopsy specimens from DLBCL of not otherwise specified (NOS) subtype with either a *BCL2* or *BCL6* rearrangement (single hit), high-grade B-cell lymphoma with *MYC* and *BCL2* or *BCL6* rearrangements (double hit), from Burkitt lymphoma (BL) as well as from non-neoplastic palatine tonsils, and non-neoplastic lymph nodes (LN), were retrieved from the archives of the Institute of Pathology, Charité-University Medicine, Berlin.

Multiple tissue arrays (MTAs) were obtained from US Biomax and contained various DLBCL specimens that were not further diagnosed according to cytogenetic rearrangements. Immunohistochemistry was performed as described in Supplementary Materials and Methods. The study involving primary human tissues was conducted according to the declaration of Helsinki and in accordance with local ethical guidelines.

Cell lines and primary B-NHL cells

The human B-NHL cell lines Su-DHL-4 and OCI-Ly7 (diffuse large B-cell lymphoma,

6

DLBCL), JeKo-1 (mantle cell lymphoma, MCL) were obtained from DSMZ (Braunschweig, Germany); Raji cells (Burkitt lymphoma, BL) were from ATCC (Manassas, VA). Upon receipt, all cell lines were expanded over 1-2 weeks and aliquots were immediately frozen in liquid nitrogen. Gene expression analysis was performed 2-3 days after thawing. Mycoplasma testing was not performed. Human umbilical vein cells (HUVEC) were purchased from Promocell (Heidelberg, Germany) and cultured in endothelial cell medium over 2-3 passages before use.

Patient-derived DLBCL and MCL xenograft samples (PDX) were obtained from Dana-Farber Cancer Institute (PRoXe depository, Boston, MA) and used after a single NOD.Cg-Prkdcscid Il2rg tm1 Wjl/SzJ (NSG) mouse passage. All primary cell lines were directly obtained from public depositories or from a commercial supplier and not additionally authenticated before use. Primary B cells (CD19$^+$ CD45$^+$ CD69$^-$ CD4$^-$ CD8$^-$ CD14$^-$ 7AAD$^-$) from healthy donors were purified from PBMCs via a Ficoll gradient and further sorted by flow cytometry.

HUVEC activation assay

HUVECs were starved overnight in serum and growth factor free endothelial basal medium (Promocell) at a cell density of $1x10^4/cm^2$ in a 24-well plate. Cell cultures were supplemented with VEGF-A$_{165}$ and VEGF-C, in addition LTα1β2 was added (all 10 ng/ml) for 24 h. For VEGF-C, a 13,5 kDa non-disulfide linked homodimeric protein consisting of two 116 amino acid polypeptide chains was chosen.

In a spheroid-based angiogenesis assay, HUVECs (at passage 3 for all experiments) were cultured for two days, trypsinized, washed in PBS and resuspended in basal medium

7

mixed with methocel stock solution (0.012 % in basal medium) in a 4:1 ratio. 25 μl cell suspension were pipetted dropwise on non-adherent culture dishes, turned upside-down to form hanging drop cultures. Collagen mix was prepared on ice using Collagen type I diluted in 10x PBS in a 4:1 ratio, pH 7. Spheroids were obtained after 24 h, mixed in methocel-collagen medium, plated in cell culture dishes and polymerized for 30 min at 37°C. Spheroids were stimulated with VEGF-A, VEGF-C, LTα1/β2 (all 25 ng/ml) and anti-VEGFR-2 antibody (50 ng/ml, clone: 89106 R&D Systems) for 24 h. Spheroids were fixed in 4 % PFA, images were recorded with transmission microscopy and sprouts were analyzed with ImageJ.

Tumor cell transfer

Single-cell suspensions were prepared and transferred i.v. exactly as described (13); at least 2–6 independent lymphoma clones derived from different Eμ-*Myc* mice were tested. Tumor load in recipient mice was determined by spleen weight, or by flow cytometric analysis. Transplantation of MCA313 primary fibrosarcoma cells was performed by subcutaneous (s.c.) injection of 1×10^6 cells in PBS.

Antibody and *in vivo* LTβR inhibitor treatment

LTβR-blocking immunoglobulin (LTβR-Ig; 100 μg; Biogen Idec) or IgG1 isotype control antibody MOPC21 was injected twice intraperitoneally (100 μg; i.p.), exactly as described (16).

Mice were injected i.p. on days 1 and 6 after Eμ-*Myc* lymphoma cell administration either with 0.8 mg rat anti-VEGFR-2 antibody (clone DC101), or with isotype control

8

IgG1 (both from BioX Cell). After fibrosarcoma transplantation, once small s.c. nodules became palpable, antibodies were injected on two occasions at 5 day intervals.

Pharmacological inhibition

The VEGFR-3 kinase inhibitor SAR131675 (SelleckChem) was dissolved in DMSO and further diluted in 0.6% methylcellulose/0.25% Tween 80. Animals were treated for 6 consecutive days with 100 mg/kg b.w. of the drug *per os,* starting at day 2 after Eμ-*Myc* lymphoma transplantation, or when fibrosarcoma became palpable.

Gene expression profiling

LN stromal cells were sorted from Wt controls and from animals transplanted with Eμ-*Myc* lymphoma cells. The average lymphoma load in LNs was 4–10% of all lymphocytes. Stromal cell purity after sorting was >95%.

For each sample, 80 ng RNA was pooled from 4–6 independent sorting experiments and reverse-transcribed using the Illumina Total Prep™ RNA Amplification Kit. The biotin-labeled transcripts were hybridized to Illumina Mouse WG-6 v2.0 Expression BeadChips and processed for detection. Differential expression was evaluated as $\log_2$ fold-change (FC). A detailed description of microarray data generation, quantitative real-time PCR and bioinformatic processing is given in Supplementary Methods and were performed essentially as previously described (16). Data are deposited under GEO repository accession number GSE126033.

9

Adoptive splenocyte transfer and transmigration assay

Splenocytes were labeled with SNARF-1 fluorescent dye (ThermoFisher), and then 3×10^7 cells per recipient mouse were injected i.v.. Four hours after cell transfer, mice were sacrificed, inguinal LNs were dissected, and cells were analyzed by flow cytometry.

***In vivo* proliferation assay**

Detection of bromodeoxyuridine (BrdU) incorporation into proliferating ECs in mice was done essentially as previously described (16).

Vessel permeability and perfusion assay

FITC-coupled dextran polymers (10, 40, and 150 kDa; all Sigma-Aldrich) diluted in PBS were injected intravenously (0.5 mg) into control, Eμ-*Myc* cell-transferred, or subcutaneously fibrosarcoma-bearing mice. Vessel perfusion was examined by i.v. injection of fluorescence-coupled Isolectin GS-IB4 (Thermo Scientific).

Inguinal LNs or fibrosarcoma tumors were fixed in 4% paraformaldehyde/PBS for immunohistology.

Statistical analysis

Statistical data were evaluated using GraphPad Prism (Version 6) software. The confidence level was 95%, with a significance level of 5% (α=0.05). Results are expressed as the arithmetic means ± SEM. Data comparison with P-values of ≤0.05 was considered statistically significant. P-values were calculated by Wilcoxon signed-rank test, Mann-Whitney U-test for non-normally distributed data, a two-tailed unpaired

10

Student's t-test for normally distributed data, or a paired Student's t-test, as indicated.

11

Results

The murine Eμ-*Myc* lymphoma model mimics human high-grade B-NHL-induced stromal angiogenesis

In human, areas of high MVD were seen in aggressive B-NHL samples (**Fig. 1A, B**). Compared with non-neoplastic tonsils or LN, the number of large vessels in the DLBCL samples was not affected, but the number of small vessels was increased 1,5–3-fold (**Fig. 1C**). These ratios were higher in high-grade B-NHL (*MYC* and *BCL2* or *BCL6* double translocated) and Burkitt lymphoma compared with single-hit DLBCL or DLBCL with unknown rearrangements. Small vessels were rarely PNAd positive (2/30 DLBCL cases), indicating that they represented a capillary phenotype, but not HEVs (**Supplementary Fig. S1**). Functionally, this lower vessel differentiation might result in impaired immigration of immunoprotective effector T cells (17).

To address the mechanisms of lymphoma-induced angiogenesis, we used transgenic Eμ-*Myc* mice that spontaneously develop lymphoma that mimic important aspects of human high-grade B-cell lymphomas (13, 18). Eμ-*Myc* lymphoma cells were transferred by i.v. injection into Wt mice. Between 9 and 12 days after lymphoma cell transfer (mean 5–15% of all CD45$^+$ cells), LNs rapidly developed a 3-fold increase in small vessels compared with an untreated cohort (**Fig. 1D, E**). This process was already visible by days 5–8, indicating that angiogenesis might be an early prerequisite for lymphoma progression. Anti-CD31 staining of LNs from spontaneously diseased Eμ-*Myc* transgenic mice with a high tumor burden revealed the occurrence of a majority of small vessels, which had substantial morphological similarities both to LNs from Eμ-*Myc* lymphoma-transplanted mice and to human DLBCL (**Fig. 1F**).

The murine Eμ-*Myc* model therefore mimics microanatomic aspects of lymphoma-induced vascular alterations that occur in human high-grade B-cell lymphoma.

Transcriptional modifications of LN vascular stromal cells occur early after Eμ-*Myc* lymphoma challenge

Stromal populations from inguinal LNs derived from mice were identified by differential expression of gp38, the adhesion molecule CD31, and the LEC marker Lyve1. The blood vasculature was clearly distinguishable from lymphatics by the absence of Lyve1 staining and, additionally, by a higher intensity staining of CD31 (**Fig. 2A**).

FRCs, LECs, and BECs were sorted from stroma-enriched fractions (CD45⁻) of pooled LNs from untreated and Eμ-*Myc* lymphoma-transplanted animals (**Fig. 2B**). Mice were sacrificed when tumor cells typically made up less than 10% of leukocytes in the LNs (days 8-12). FRCs exhibited the highest gene expression of the chemokines *Ccl19, Ccl21*, and of *Il7*. BECs expressed a high level of ESAM, and LECs expressed the marker gene *Lyve1* (**Fig. 2C, D**). Using whole transcriptome GEP relative changes in gene expression from untreated stromal cells were compared with those from lymphoma-challenged mice. Subset-specific expression of the expected gene markers was confirmed (**Supplementary Fig. S2A**). Gene expression of lymphoma B cell specific genes, such as *Ptprc* (CD45R/B220), *Ms4a1* (CD20) and *Cxcr5* within data sets from stromal subsets was rigorously excluded (**Supplementary Fig. S2B**).

In all three subsets, there were significant overall differences in expression between the treated and untreated mice (**Fig. 2E**). A total of 710 genes were selectively upregulated in lymphoma-exposed cells. An overlap of 114 genes that were upregulated in all three

13

subpopulations occurred (**Fig. 2F, G**). Tumor induction and progression has been linked to a chronic type of inflammatory milieu. Therefore, we explored whether lymphoma-dependent stromal cells showed expression of genes characteristic of a LN-specific inflammation signature (8) (https://www.ncbi.nlm.nih.gov/geo/query/acc.cgi?acc=GSE15907). Unexpectedly, no significant upregulation of inflammation signature genes was observed (**Supplementary Fig. S2C, D**).

On the other hand, similar to an inflammatory condition, gene ontology (GO) analysis (**Supplementary Table S1A**) as well as GSEA confirmed enriched signatures related to proliferation and cell cycle in all three stromal cell subsets (**Supplementary Fig. 3A–C; Supplementary Table S1B**). Phenotypically, the proportion of BECs, LECs and FRCs in S-phase (EdU$^+$) was substantially higher than in those from untreated LNs (**Supplementary Fig. 3D**). Collectively, the angiogenic switch in lymphoma-bearing LNs is characterized by proliferation of BECs. Gene expression and proliferation data confirmed the role of lymphangiogenesis during lymphoma progression. Lymphangiogenesis has been established as a structural pathogenetic factor supporting lymph flow and lymphoma dissemination (9, 19-21).

As an indication of structural alterations, in FRCs the KEGG gene sets correlated with 'Collagen_Formation' and 'Extracellular_Matrix_Organization' were significantly enriched with downregulated genes (**Supplementary Table S1B**). Both signatures contain genes (e.g., *Collagen genes; Timp1*, *2*) that determine the formation and stability of the ECM. Among other functions that sustain tissue homeostasis, one important function of the ECM includes VEGF-A gradient shaping and integrin signaling, which

14

are both involved in regulating the balance between stalk cell proliferation and tip cell migration in the formation of the vascular branches (22). Thus, this signature may indicate a perturbance of ECM function regarding guidance of angiogenesis.

BECs assemble into microvessels associated with a negative clinical prognosis, thus we focused on blood vessels in greater detail.

Regulation of a pro-angiogenic milieu in Eμ-*Myc* lymphoma-bearing LNs involves noncanonical pathways

Inguinal LNs were removed when tumor load was low (5–10% of all CD45$^+$ cells) or medium (10–15%), RNA was extracted and analyzed using angiogenesis gene-specific qRT-PCR arrays (**Fig. 3A**). With a medium tumor load, among the strongest upregulation of mRNA compared to non-tumor bearing LNs was noted for *Vegf-c* (>4-fold); VEGF-C is a ligand for VEGFR-2 and VEGFR-3, and functions as a growth factor for lymphangiogenesis and for BECs (23).

GEP on non-transformed follicular B cells derived from control mice and Eμ-*Myc* lymphoma cells from transplanted mice was performed. The latter exhibited gene sets characteristically upregulated in human DLBCL as well (FC>1, p<0.05; **Supplementary Fig. S4A, B**). Applying an angiogenesis-related GSEA signature, several strong immunomodulators and pro-angiogenic factors were found to be substantially upregulated in lymphoma cells. This list contained genes encoding secreted proteins such as *Lgals1* (Galectin-1) and *Lgals9* (Galectin-9) involved in suppressing T lymphocytes and niche formation (**Fig. 3B**) (24).

15

Vascular remodeling at the disease onset was analyzed by confocal microscopy on thick tissue sections (100 μm). Because transplanted Eμ-*Myc* lymphoma cells home preferentially to the paracortical T-cell zone of LNs in a CCR7-dependent manner, we co-stained the T-cell area (CD3^{+}) and quantified the CD31^{+} 3D-surface area within it. LECs (Lyve1^{+}) were largely absent from the paracortical T-cell zone, however they were also found to be expanded (**Supplementary Fig. S4C**, **Fig. 3D**). Lymphoma induced an expansion of HEVs in the LNs of both the Eμ-*Myc* transgenic and transplanted animals, and they had many more small vessels and capillaries extending into the T-cell zone than control LNs (**Fig. 3C, D**).

During sprouting angiogenesis, growing capillaries are spearheaded by specialized ECs termed 'tip cells' (25, 26). We analyzed the BEC-specific gene expression from lymphoma-challenged LNs against a refined signature of tip cell genes; however, no strong enrichment with respect to the BEC-specific ranking of genes was found (**Fig. 3E; Supplementary Fig. S4D**). Likewise, the KEGG 'VEGF Signaling Pathway', which relates to VEGF-A/VEGFR-2-induced signaling, was not enriched (**Fig. 3F; Supplementary Fig. S4E**). In contrast, a gene signature of distinct transcriptional responses to VEGF-C/VEGFR-3 stimulation was modestly enriched among the top 10 genes up- or downregulated in BECs (**Fig. 3G**) (27).

GSEA indicated a significant enrichment of genes downregulated by the hypoxia-related *HIF-1α* gene among the genes upregulated in BECs (**Fig. 3H**), suggesting a lack of activation of this signaling route. Tissue staining using the hypoxia marker pimonidazole was negative in LNs from lymphoma-transplanted mice and scant in LNs from Eμ-*Myc* transgenic mice, which was in striking contrast to the marked hypoxia demonstrated in

16

subcutaneously grown fibrosarcoma tissue (**Supplementary Fig. S4F**). A Notch target gene signature was downregulated in BECs (**Fig. 3I**), indicating the lack of a Notch-dependent feedback loop from tip to stalk cells.

A stem cell transcriptional pattern was enriched among the BEC-specific genes. A 'Stemness signature' (28) of 100 genes was selected, 35 of which were upregulated (FC>1; p≤0.001) among the BEC-specific genes (**Fig. 3J**). Genes related to spindle assembly and kinetochore formation, e.g., *Bub1*, *Mad2l1*, and *Nusap1*, were significantly different. The forkhead TF *Foxm1*, which binds to the majority of kinetochore and cell division gene promoters (29), was upregulated (FC=2.6), indicating that it has a coordinating function in lymphoma-induced BEC reprogramming.

Eμ-*Myc* lymphoma induces aberrant tip cell and filopodia formation in LNs

We visualized ECs in LNs from tamoxifen-inducible *Cdh5-GFP* reporter mice. The vascular surface area increased 2-fold upon lymphoma induction. Correspondingly, vessel length increased about 2-fold (mean control: 16.687 μm; mean *Eμ-Myc*: 32.767 μm; P=0.05). A complex vascular network intermingled with dense loops with smaller diameters, and concomitantly, a 3-fold increased frequency of branching points was seen (**Fig. 4A-C**). However, upon normalization of vessel length, distances between branches and loops were not significantly changed, indicating that the leading morphological effect was an increase in vascular density. The isolectin GS-IB4 was infused systemically. Perfused vessels were quantified using the ratio of all double-stained IB4^{+}/GFP^{+} vessels relative to all GFP^{+} vessels. In total, about 80% of the vasculature was found to be open for intraluminal flow (**Fig. 4D**).

17

Blood vessels of lymphoma-challenged and untreated LNs were mainly impervious to fluorescent 10, 40 and 150 kDa dextrans, whereas vessels in fibrosarcoma tissue leaked 10 and 40 kDa forms (**Supplementary Fig. S5A-C**). Additionally, mice were inoculated with Eμ-*Myc* B cells, and then transplanted with SNARF-1-labeled splenocytes. Total numbers of CD4$^+$ and CD8$^+$ T cells, monocytes (CD11b$^+$), and B lymphocytes (B220$^+$) were about 2-fold higher in lymphoma-bearing LNs (**Supplementary Fig. S5D**).

In *Cdh5-GFP* mice lymphoma-exposed LNs exhibited numerous slender filopodial bursts that emanated from the lateral sides of vessels, but only rarely extended from the leading edge where tip cells are usually located (**Fig. 4E**). Several cellular protrusions reminiscent of blebs normally associated with apoptosis, cell migration, and division in ontogeny (30, 31) were observed. Next, to explore tip cell occurrence further anti-Esm1 immunostainings were performed (**Fig. 4F**). Esm1 expression was found to be EC (Cdh5-GFP$^+$) restricted, but rather distributed throughout the blood vasculature. This pattern is consistent with the observation that Esm1 expression is restricted to tip cells in the retina, but widely distributed throughout carcinoma vasculature with a disturbance of the VEGF-A gradient (32). The Notch ligand Dll4 was variably expressed in ECs with filopodia (**Supplementary Fig. S5E**). Collectively, disseminated localization of Esm1$^+$ sprouting ECs together with variable Dll4 expression are distinguishable from highly ordered morphologies and functions of tip cells in developing organs.

LTβR signaling is required for Eμ-*Myc* lymphoma-induced angiogenesis in LNs

To determine the role of LTβR-LTαβ signaling, we transplanted B cells from Eμ-*Myc* and Eμ-*Myc* × *Ltα$^{-/-}$* mice. Using a cell cycle gene-specific qRT-PCR array, we found

18

34/78 genes upregulated in Eμ-*Myc* lymphoma-exposed BECs (**Fig. 5A**). By contrast, this proliferation signature was not obtained when *Ltα*-deficient Eμ-*Myc* lymphoma cells were transplanted (4/78 genes upregulated; **Fig. 5B**).

When Eμ-*Myc* lymphoma-bearing mice received the inhibitory decoy receptor protein LTβR-Ig, a significant delay in the growth of lymphoma was observed. Additionally, the vascular surface area (CD31$^+$) and the proliferation rate (BrdU$^+$) of BECs were almost normalized to those from control mice (**Fig. 5C–F**). In lymphoma-bearing *Cdh5-GFP* mice, the dense and hyperplastic GFP$^+$ vasculature was not visible when animals were LTβR-Ig-treated (**Fig. 5G**); in particular, the number of branching points was about half that in controls (**Fig. 5H, I**); loss of cuboid ECs with a concomitant decrease in luminal PNAd staining was confirmed (**Supplementary Fig. S6A**).

To exclude that the growth reduction was caused by indirect effects on other LTβR-expressing cell populations (33), *Cdh5-cre/ERT2* × *LtβR$^{fl/fl}$* mice were generated. Reduction in LTβR expression in BECs from tamoxifen-treated mice was confirmed by flow cytometry (**Supplementary Fig. S6B, C**). After administration of lymphoma cells, a substantial decrease in CD31$^+$ vascular surface area, tumor load and ICAM1 expression was observed compared with *Cdh5-cre/ERT2* controls (**Fig. 5J, K**; **Supplementary Fig. S6D**).

VEGFR-3 signaling is induced by lymphoma growth and stimulates LN angiogenesis

We examined the growth kinetics of Eμ-*Myc* lymphoma in mice treated with a blocking anti-VEGFR-2 antibody. Compared with controls, similar lymphoma growth rates,

19

identical vascular surface areas (CD31$^+$), as well as branching points were obtained in lymphoma-exposed LNs (**Fig. 6A, B, C**). By contrast, anti-VEGFR-2 antibody treatment caused a substantial tumor and vascular growth retardation in subcutaneously grown fibrosarcoma (**Supplementary Fig. S7A, B, C**).

Next, we separated LN stromal cell subsets, Eμ-*Myc* lymphoma cells, and non-transformed leukocytes. Upregulation of *Vegfc* was seen in FRCs, but the strongest gene expression was seen in the lymphoma B cells (**Fig. 6D)**. *Vegfd* gene expression was reduced (**Supplementary Figure S7D**). Correspondingly, VEGF-C serum levels were much higher in Eμ-*Myc* mice (**Fig. 6E**). In accordance, several human lymphoma cell lines and the patient-derived lymphoma samples (PDX) expressed much higher *VEGFA* and *VEGFC* mRNAs compared to normal B cells (**Supplementary Fig. S7E**).

Stimulation of spheroid-grown human umbilical vein ECs (HUVEC) by VEGF-C induced sprouts at lower rate than treatment with VEGF-A (**Fig. 6F**). Although LTα1β2 alone had no stimulatory effect on sprouting, the combination with VEGF-C revealed a synergistic growth effect (mean 25%). This effect was not seen in the combination of LTα1β2 with VEGF-A (**Fig. 6F**). Stimulation of HUVECs with VEGF-C caused a strong VEGFR-3 downregulation, which could be substantially ameliorated by a concomitant LTα1β2 stimulation (**Fig. 6G**). We conclude that LTβR signaling might interfere with VEFR-3 endocytosis or recycling, a general mechanism of receptor tyrosine kinase regulation (34).

In whole-tissue homogenates from lymphoma-bearing LNs, a 4-fold upregulation of VEGF-C protein expression was detected. The active variant of the VEGF-C protein is generated after enzymatic cleavage of a propeptide. Upon lymphoma challenge, there

20

was increased conversion to the mature protein in spleen and LNs, indicating that lymphoma had induced enzymatic activities necessary for generating biologically active VEGF-C (**Fig. 6H, I**). Gene expression of collagen- and calcium-binding EGF domains 1 (*Ccbe1*) was strongly enhanced in Eμ-*Myc* lymphoma cells, but not in LN stroma (**Fig. 6J**). CCBE1 protein localizes together with pro-VEGF-C and ADAMTS3 on ECM and EC surfaces, where a cleavage complex is assembled allowing the mature VEGF-C to activate VEGFR-3 (35). Importantly, fully processed VEGF-C is not only lymphangiogenic, but also angiogenic (36, 37).

VEGFR-3 is activated by VEGF-C and -D and is highly expressed in leading-edge ECs that undergo sprouting (38). We detected *Vegfr3* gene expression in BECs and LECs already in steady-state conditions, and observed a 2-fold induction in *Vegfr3* expression in LECs upon lymphoma challenge (**Fig. 6K**). This upregulation is consistent with VEGFR-3 signaling in LECs as a driving force for lymphangiogenesis. *Vegfr2* mRNA was upregulated in LECs and BECs, which corresponded to a modest increase in VEGFR-2 protein expression on BECs, but not in LECs (**Supplementary Fig. S7F, G**). To confirm the VEGFR-3 specific pro-proliferative activity *in vitro*, HUVECs grown in spheroids were treated with VEGF-A, VEGF-C and LTα1β2. In the presence of a VEGFR-2 blocking antibody, VEGF-C plus LTα1β2 still stimulated the formation of sprouts, which was abrogated in the combination of VEGF-A and LTα1β2 (**Supplementary Fig. S7H**). Next, inducible *Vegfr3-GFP* reporter mice (*Tg(Flt4-tm2.1-cre ERT2) Rosa26-mTmG*) were transplanted with lymphoma cells. The highest frequency of GFP signal was found in LECs, followed by BECs, as confirmed by anti-VEGFR3 antibody detection (**Fig. 6L; Supplementary Fig. S7I**). We conclude that *in*

21

vivo even a small population of VEGFR-3 carrying BECs can gain a leading role in lymphoma-induced angiogenesis, independent from VEGFR-2 activity.

Treatment with the VEGFR-3 kinase inhibitor SAR131675, which has a much higher selectivity for VEGFR-3 than for VEGFR-1/2, inhibited both lymphoma progression and vascular expansion stimulated by lymphoma (**Fig. 6M**). A direct anti-lymphoma effect of the drug was excluded since spleen located Eμ-Myc cells were spared (**Supplementary Fig. S7J)**. Concomitantly, expansion of the lymphatic vasculature (Lyve1$^+$) was retarded (**Supplementary Fig. S7K, L**). Treatment with another VEGFR-3 kinase inhibitor, MAZ51 decreased the density of the vascular surface (CD31$^+$) in the T-cell zone 0.5-fold (**Supplementary Fig. S7M**). In fibrosarcoma, SAR131675 had no effect on tumor development **(Figure 6N**).

Taken together, VEGFR-3$^+$ BECs in angiogenic vessels sensitized the vasculature for proliferation and differentiation inhibition by specific kinase inhibitors.

22

Discussion

We elucidated the mechanisms regulating the angiogenic switch and the morphogenesis of new blood vessels in aggressive B-cell lymphoma. Using the transgenic Eμ-*Myc* mouse model, we detected a substantial morphological similarity with human aggressive lymphoma characterized by a high MVD, a feature that has an adverse prognostic impact on patient survival (2, 3). Lymphoma B cells provide growth stimuli that induce a marked proliferation of BECs. This lymphoma cell crosstalk with BECs in turn translates to vessel hypersprouting and capillary growth.

The clinical importance of angiogenesis for growth of solid tumors is well-recognized (39) (4, 40). Therapeutic concepts from solid tumors targeting the VEGF-A/VEGFR-1/2 axis have been adopted for DLBCL and mantle cell lymphoma combination therapies, resulting in rather disappointing clinical outcomes (6, 7). Here, we show that BEC proliferation and angiogenesis proceeded in a VEGFR-2-independent manner, a finding that would not have been anticipated from precedents set from studies of solid malignancies. Instead, we identified VEGFR-3 as the leading mediator of blood vessel expansion, a signaling process fueled by lymphoma cell- and FRC-derived VEGF-C. Although a much smaller fraction of BECs than LECs expressed VEGFR-3, treatment with VEGFR-3 inhibitors was sufficient to normalize angiogenesis and attenuate lymphoma expansion.

It is worthy to note that a limitation of pharmacological inhibitor administration to block receptor tyrosine kinase activity is the specificity of their activity. Selectivity of VEGFR-3 drug targeting might vary with the active concentration of SAR131675, MAZ51 or any other tyrosine kinase inhibitor, respectively (41). In addition, ligand-independent

23

activation of VEGFR-3 in angiogenesis may lead to inefficiency of an anti-VEGFR-3 antibody treatment (42). In contrast, a BEC-specific genetic deletion of the VEGFR-3 would allow more definite conclusions regarding the mechanism of lymphoma-induced angiogenesis. Here, we chose drug application in our animal model which has the potential to reveal a therapeutic solution directly translatable into clinical studies.

The overexpression of the VEGFR-3 ligands VEGF-C by lymphoma cells and macrophages was interpreted to be the inducer of the lymphatic vasculature, but not of blood vessels (9, 21, 43). The VEGF-C /VEGFR-3 axis is important for lymphatic sinus growth and increased lymph flow that correlated with metastasis of solid tumors and lymphoma cell dissemination, respectively (19, 41). By contrast, we showed previously that the preferred dissemination route of transplanted Eμ-*Myc* B cells involves the LN T-cell zone, which can be accessed via HEVs (13). We also demonstrate structural remodeling and transcriptional reprogramming of lymphoma-exposed BECs, which are the major structural constituents of microvessels. To bring lymphangiogenesis and blood vessel growth in agreement, we envision that our i.v. transfer model reports on early steps of lymphoma B cell homing and niche formation. These early steps are decisive for further LN remodeling and subsequently, lymphatic sinus growth and lymphoma cell dissemination. In LN, lymphatic and blood vasculature growth proceed in a VEGFR-3 dependent manner.

Our results draw parallels with infections and solid tumors, but they also reveal clear distinctions from both. In clear contrast to many solid tumors and their LN metastasis, lymphoma-challenged BECs acquired gene signatures that were not enriched for *Notch*, *Vegfa* or *Hif-1α* pathway genes. LN remodeling in inflammation proceeds in sequential

24

overlapping phases (12, 15, 44). In the initiation phase a rapid blood vasculature growth is dependent on IL-1β secreting DCs that stimulate VEGF-A release from FRCs (45). In contrast, we here examined LN from lymphoma challenged mice at days 8-12, when VEGF-A has likely declined and instead, VEGF-C has gained a leading role.

The TF HIF-1α is induced by hypoxia and functions as the main transcriptional regulator of tumor-associated vascular remodeling (46). In conjunction with the weak pimonidazole staining seen in lymphoma-bearing LNs, our data point to a micromilieu in which hypoxia is not a driving force for angiogenesis. We conclude that LNs have a distinct vascular microanatomy that involves highly specialized HEVs and capillaries that can accommodate an autochthonous tumor without changing the tissue-specific oxygen metabolism.

Consistent with the inflammatory response upon infection, Eμ-*Myc* lymphoma-challenged LNs rapidly begin HEV remodeling (15, 33). One study shows that blocking VEGF-A or its cognate receptor VEGFR-2 does not inhibit LCMV-induced vascular expansion in LNs (15). This observation parallels a mechanism that we detected in lymphoma-induced angiogenesis; we also could not find evidence for a functional role of VEGF-A in this process. During viral infection, B cell-derived LTα1β2 contributes to remodeling of the HEV network in the acute phase (15). The infection model examined the role of activated B cells in an environment perturbed by virus-induced structural disruption of the reticular network. In the present study, LT-expressing lymphoma B cells were being added to a largely intact LN microstructure. Thus, a functional B cell-dependent LTα1β2-LTβR signaling loop was present. Immunopharmacological interference with LTβR signaling on BECs retarded angiogenesis substantially and

25

delayed progression of B-cell lymphoma. Although LTα1β2 did not induce HUVEC proliferation and sprouting alone, we envision that it acts as a morphogen stimulating HEV or capillary branching and thus, may synergize with the growth factor VEGF-C.

Interestingly, VEGF-D overexpressing tumor cells induced downregulation of BMP-4 in HEV cells (47). Loss of BMP-4 expression resulted in severe remodeling of HEVs, in contrast to our lymphoma model a key mediator of this process, VEGF-D, was not increased in tumor-exposed LN. Likewise, BMP-4 gene expression in BECs was not significantly altered, indicating that these linked pathogenetic factors are unlikely to cooperate in lymphoma-induced vascular remodeling.

We note that branching points after LTβR-Ig treatment were strongly diminished. Regarding the hierarchy of this interaction, it has been shown that LTβR stimulation of murine FRC-type cells upregulates VEGF expression, suggesting that the LTβR-LTα1β2 axis on FRCs regulates VEGF levels and thus, EC proliferation (44).

Despite large similarities to infection-induced LN remodeling, we note that inflammation is not the cause for our observations. A comparison of our transcriptome dataset with microarray data from published results characterizing stromal response to inflammation showed no enrichment of an inflammation signature (8).

Morphological analysis revealed a hypersprouting phenotype of lymphoma-associated vessels. GSEA of BECs did not indicate an enrichment of a tip cell or Notch signaling pathway gene signature, which would have been expected from ontogeny or other tumor angiogenesis models (48-50). Angiogenic sprouting is led by tip cells that sense a VEGF-A guide cue and produce Dll4. This Notch ligand acts on stalk cells preceding the tip that proliferate but are prevented from adopting a tip cell differentiation (22). It has also been

26

shown that VEGFR-3 localizes in endothelial sprouts of several solid tumors and in the developing mouse retina in leading tip cells. In the absence of VEGFR-2 activity, VEGFR-3-transmitted signals can sustain some degree of angiogenesis (38). When Notch signaling is disrupted, increased sprouting in conjunction with induced *Vegfr3* expression occurs (51). We note that Esm1 and Dll4 expression normally associated with a tip cell phenotype was irregular in lymphoma vasculature, contrasting to studies in highly ordered developing tissues like retina (42, 49, 52). Thus, in mice unopposed VEGFR-3 activity that is released from a Notch signaling brake can result in a hyperactive sprouting phenotype, as seen in our Eμ-*Myc* lymphoma model.

In summary, we showed that lymphoma angiogenesis proceeds in unique transcriptional and morphogenic programs, which are clearly distinct from solid tumor and inflammation-induced structural remodeling. Identification of the VEGFR-3 and the LTβR signaling pathways as regulators of lymphoma angiogenesis strongly suggests that combinatorial therapies targeting vessel densities should be reconsidered.

27

Acknowledgements

We thank Daniel Besser (MDC) for help in bioinformatic analysis; Christian Friese (Charité, Berlin) for expert technical assistance; Anje Sporbert, Matthias Richter for microscopic image analysis (Advanced Light Microscopy Platform; MDC); Ralf Adams (MPI, Münster, Germany) and Taija Mäkinen (Uppsala University, Sweden) for Cre-deleter mouse strains.

28

References

1.   Lenz G, Wright G, Dave SS, Xiao W, Powell J, Zhao H, et al. Stromal gene signatures in large-B-cell lymphomas. N Engl J Med. 2008;359:2313-23.

2.   Cardesa-Salzmann TM, Colomo L, Gutierrez G, Chan WC, Weisenburger D, Climent F, et al. High microvessel density determines a poor outcome in patients with diffuse large B-cell lymphoma treated with rituximab plus chemotherapy. Haematologica. 2011;96:996-1001.

3.   Ganjoo KN, Moore AM, Orazi A, Sen JA, Johnson CS, An CS. The importance of angiogenesis markers in the outcome of patients with diffuse large B cell lymphoma: a retrospective study of 97 patients. J Cancer Res Clin Oncol. 2008;134:381-7.

4.   Carmeliet P, Jain RK. Angiogenesis in cancer and other diseases. Nature. 2000;407:249-57.

5.   Kerbel R, Folkman J. Clinical translation of angiogenesis inhibitors. Nat Rev Cancer. 2002;2:727-39.

6.   Ganjoo KN, An CS, Robertson MJ, Gordon LI, Sen JA, Weisenbach J, et al. Rituximab, bevacizumab and CHOP (RA-CHOP) in untreated diffuse large B-cell lymphoma: safety, biomarker and pharmacokinetic analysis. Leuk Lymphoma. 2006;47:998-1005.

7.   Seymour JF, Pfreundschuh M, Trneny M, Sehn LH, Catalano J, Csinady E, et al. R-CHOP with or without bevacizumab in patients with previously untreated diffuse large B-cell lymphoma: final MAIN study outcomes. Haematologica. 2014;99:1343-9.

8.   Malhotra D, Fletcher AL, Astarita J, Lukacs-Kornek V, Tayalia P, Gonzalez SF, et al. Transcriptional profiling of stroma from inflamed and resting lymph nodes defines immunological hallmarks. Nat Immunol. 2012;13:499-510.

9.   Song K, Herzog BH, Sheng M, Fu J, McDaniel JM, Chen H, et al. Lenalidomide inhibits lymphangiogenesis in preclinical models of mantle cell lymphoma. Cancer Res. 2013;73:7254-64.

10.   Ruan J, Luo M, Wang C, Fan L, Yang SN, Cardenas M, et al. Imatinib disrupts lymphoma angiogenesis by targeting vascular pericytes. Blood. 2013;121:5192-202.

11.   Hopken UE, Rehm A. Homeostatic chemokines guide lymphoma cells to tumor growth-promoting niches within secondary lymphoid organs. J Mol Med (Berl). 2012;90:1237-45.

12.   Webster B, Ekland EH, Agle LM, Chyou S, Ruggieri R, Lu TT. Regulation of lymph node vascular growth by dendritic cells. J Exp Med. 2006;203:1903-13.

13.   Rehm A, Mensen A, Schradi K, Gerlach K, Wittstock S, Winter S, et al. Cooperative function of CCR7 and lymphotoxin in the formation of a lymphoma-permissive niche within murine secondary lymphoid organs. Blood. 2011;118:1020-33.

14.   Onder L, Danuser R, Scandella E, Firner S, Chai Q, Hehlgans T, et al. Endothelial cell-specific lymphotoxin-beta receptor signaling is critical for lymph node and high endothelial venule formation. J Exp Med. 2013;210:465-73.

15.   Kumar V, Scandella E, Danuser R, Onder L, Nitschke M, Fukui Y, et al. Global lymphoid tissue remodeling during a viral infection is orchestrated by a B cell-lymphotoxin-dependent pathway. Blood. 2010;115:4725-33.

16.   Heinig K, Gatjen M, Grau M, Stache V, Anagnostopoulos I, Gerlach K, et al. Access to follicular dendritic cells is a pivotal step in murine chronic lymphocytic leukemia B-cell activation and proliferation. Cancer Discov. 2014;4:1448-65.

17.   Hindley JP, Jones E, Smart K, Bridgeman H, Lauder SN, Ondondo B, et al. T-cell trafficking facilitated by high endothelial venules is required for tumor control after regulatory T-cell depletion. Cancer Res. 2012;72:5473-82.

18.   Reimann M, Lee S, Loddenkemper C, Dorr JR, Tabor V, Aichele P, et al. Tumor stroma-derived TGF-beta limits myc-driven lymphomagenesis via Suv39h1-dependent senescence. Cancer Cell. 2010;17:262-72.

19.   Habenicht LM, Kirschbaum SB, Furuya M, Harrell MI, Ruddell A. Tumor Regulation of Lymph Node Lymphatic Sinus Growth and Lymph Flow in Mice and in Humans. Yale J Biol Med. 2017;90:403-15.

20.   Ruddell A, Mezquita P, Brandvold KA, Farr A, Iritani BM. B lymphocyte-specific c-Myc expression stimulates early and functional expansion of the vasculature and lymphatics during lymphomagenesis. Am J Pathol. 2003;163:2233-45.

21.   Ruddell A, Harrell MI, Furuya M, Kirschbaum SB, Iritani BM. B lymphocytes promote lymphogenous metastasis of lymphoma and melanoma. Neoplasia. 2011;13:748-57.

22.   Mettouchi A. The role of extracellular matrix in vascular branching morphogenesis. Cell Adh Migr. 2012;6:528-34.

23.   Alitalo K, Tammela T, Petrova TV. Lymphangiogenesis in development and human disease. Nature. 2005;438:946-53.

24.   Lykken JM, Horikawa M, Minard-Colin V, Kamata M, Miyagaki T, Poe JC, et al. Galectin-1 drives lymphoma CD20 immunotherapy resistance: validation of a preclinical system to identify resistance mechanisms. Blood. 2016;127:1886-95.

25.   del Toro R, Prahst C, Mathivet T, Siegfried G, Kaminker JS, Larrivee B, et al. Identification and functional analysis of endothelial tip cell-enriched genes. Blood. 2010;116:4025-33.

26.   Gerhardt H, Golding M, Fruttiger M, Ruhrberg C, Lundkvist A, Abramsson A, et al. VEGF guides angiogenic sprouting utilizing endothelial tip cell filopodia. J Cell Biol. 2003;161:1163-77.

27.   Dieterich LC, Ducoli L, Shin JW, Detmar M. Distinct transcriptional responses of lymphatic endothelial cells to VEGFR-3 and VEGFR-2 stimulation. Sci Data. 2017;4:170106.

28.   Shats I, Gatza ML, Chang JT, Mori S, Wang J, Rich J, et al. Using a stem cell-based signature to guide therapeutic selection in cancer. Cancer Res. 2011;71:1772-80.

29.   Thiru P, Kern DM, McKinley KL, Monda JK, Rago F, Su KC, et al. Kinetochore genes are coordinately up-regulated in human tumors as part of a FoxM1-related cell division program. Mol Biol Cell. 2014;25:1983-94.

30.   Gebala V, Collins R, Geudens I, Phng LK, Gerhardt H. Blood flow drives lumen formation by inverse membrane blebbing during angiogenesis in vivo. Nat Cell Biol. 2016;18:443-50.

31.   Reichman-Fried M, Raz E. Blood, blebs and lumen expansion. Nat Cell Biol. 2016;18:366-7.

30

32.   Rocha SF, Schiller M, Jing D, Li H, Butz S, Vestweber D, et al. Esm1 modulates endothelial tip cell behavior and vascular permeability by enhancing VEGF bioavailability. Circ Res. 2014;115:581-90.

33.   Lu TT, Browning JL. Role of the Lymphotoxin/LIGHT System in the Development and Maintenance of Reticular Networks and Vasculature in Lymphoid Tissues. Front Immunol. 2014;5:47.

34.   Lemmon MA, Schlessinger J. Cell signaling by receptor tyrosine kinases. Cell. 2010;141:1117-34.

35.   Jha SK, Rauniyar K, Karpanen T, Leppanen VM, Brouillard P, Vikkula M, et al. Efficient activation of the lymphangiogenic growth factor VEGF-C requires the C-terminal domain of VEGF-C and the N-terminal domain of CCBE1. Sci Rep. 2017;7:4916.

36.   Joukov V, Sorsa T, Kumar V, Jeltsch M, Claesson-Welsh L, Cao Y, et al. Proteolytic processing regulates receptor specificity and activity of VEGF-C. EMBO J. 1997;16:3898-911.

37.   Rauniyar K, Jha SK, Jeltsch M. Biology of Vascular Endothelial Growth Factor C in the Morphogenesis of Lymphatic Vessels. Front Bioeng Biotechnol. 2018;6:7.

38.   Tammela T, Zarkada G, Wallgard E, Murtomaki A, Suchting S, Wirzenius M, et al. Blocking VEGFR-3 suppresses angiogenic sprouting and vascular network formation. Nature. 2008;454:656-60.

39.   Hanahan D, Folkman J. Patterns and emerging mechanisms of the angiogenic switch during tumorigenesis. Cell. 1996;86:353-64.

40.   Tabchi S, Blais N. Antiangiogenesis for Advanced Non-Small-Cell Lung Cancer in the Era of Immunotherapy and Personalized Medicine. Front Oncol. 2017;7:52.

41.   Hsu MC, Pan MR, Hung WC. Two Birds, One Stone: Double Hits on Tumor Growth and Lymphangiogenesis by Targeting Vascular Endothelial Growth Factor Receptor 3. Cells. 2019;8.

42.   Benedito R, Rocha SF, Woeste M, Zamykal M, Radtke F, Casanovas O, et al. Notch-dependent VEGFR3 upregulation allows angiogenesis without VEGF-VEGFR2 signalling. Nature. 2012;484:110-4.

43.   Lohela M, Bry M, Tammela T, Alitalo K. VEGFs and receptors involved in angiogenesis versus lymphangiogenesis. Curr Opin Cell Biol. 2009;21:154-65.

44.   Chyou S, Ekland EH, Carpenter AC, Tzeng TC, Tian S, Michaud M, et al. Fibroblast-type reticular stromal cells regulate the lymph node vasculature. J Immunol. 2008;181:3887-96.

45.   Benahmed F, Chyou S, Dasoveanu D, Chen J, Kumar V, Iwakura Y, et al. Multiple CD11c+ cells collaboratively express IL-1beta to modulate stromal vascular endothelial growth factor and lymph node vascular-stromal growth. J Immunol. 2014;192:4153-63.

46.   Bristow RG, Hill RP. Hypoxia and metabolism. Hypoxia, DNA repair and genetic instability. Nat Rev Cancer. 2008;8:180-92.

47.   Farnsworth RH, Karnezis T, Shayan R, Matsumoto M, Nowell CJ, Achen MG, et al. A role for bone morphogenetic protein-4 in lymph node vascular remodeling and primary tumor growth. Cancer Res. 2011;71:6547-57.

31

48.   Cao Z, Ding BS, Guo P, Lee SB, Butler JM, Casey SC, et al. Angiocrine factors deployed by tumor vascular niche induce B cell lymphoma invasiveness and chemoresistance. Cancer Cell. 2014;25:350-65.
49.   Hellstrom M, Phng LK, Hofmann JJ, Wallgard E, Coultas L, Lindblom P, et al. Dll4 signalling through Notch1 regulates formation of tip cells during angiogenesis. Nature. 2007;445:776-80.
50.   Ridgway J, Zhang G, Wu Y, Stawicki S, Liang WC, Chanthery Y, et al. Inhibition of Dll4 signalling inhibits tumour growth by deregulating angiogenesis. Nature. 2006;444:1083-7.
51.   Siekmann AF, Lawson ND. Notch signalling limits angiogenic cell behaviour in developing zebrafish arteries. Nature. 2007;445:781-4.
52.   Suchting S, Freitas C, le Noble F, Benedito R, Breant C, Duarte A, et al. The Notch ligand Delta-like 4 negatively regulates endothelial tip cell formation and vessel branching. Proc Natl Acad Sci U S A. 2007;104:3225-30.

Figure Legends

Figure 1. Murine Eμ-*Myc* B cell lymphoma phenocopy high microvessel density in human DLBCL and Burkitt lymphoma

A) Anti-CD31 staining of non-neoplastic tonsils and DLBCL. **B)** Anti-CD34 staining on single tissue sections or on MTAs from high-grade B cell lymphoma subtypes (n.SLO: non-neoplastic lymph nodes, n=11; tonsils, n=5; DLBCL, NOS without cytogenetic data (mix), n=36; DLBCL (single hit), n=13; high-grade B cell lymphoma (double hit), n=3; Burkitt lymphoma, n=8); 3 low power fields per case and tissue slide were counted. **C)** Vessels were grouped according their sizes; small < 30 μm, and large > 30 μm. **D)** Wt mice (n>10) were adoptively transferred with Eμ-*Myc* lymphoma cells i.v.. At least 3 clones were used. Recipients were sacrificed early, day 5-8 (low tumor load, n=6) and late, day 9-12 (medium; n=5; control n=4). LNs stained with an anti-CD31 antibody (day 9). One to four sections per LN were quantitatively evaluated. **E)** Vessels were grouped as in **C). F)** LN from control mice (n=3) and from diseased transgenic Eμ-*Myc* transgenic mice (n=4) were stained as in **D),** inset shows amplification of MVDs in lymphoma bearing animals. In **C)** and **E)**, the ratios between small and large vessels are represented, error bars indicate mean ± SEM; Student's t-test. Scale bar, 100 μm. Asterisks indicate statistical significance. *, P≤0.01; **, P≤0.01; ***, P≤0.001

Figure 2. Lymph node vascular stroma cell response to Eμ-*Myc* lymphoma challenge

33

A) Immunofluorescent staining of inguinal LN sections. Images were recorded by confocal microscopy. Scale bar, 500 μm. A higher magnification of a marked area is shown on the right; scale bar 20 μm.

B) Flow cytometry sorting strategy for the isolation of the vascular stromal cell subsets FRCs (gp38$^+$ CD31$^-$), LECs (gp38$^+$ CD31$^+$), and BECs (gp38$^-$ CD31$^+$) from CD45$^-$ Ter119$^-$ stromal cell enriched fractions of pooled LNs. Data are representative of at least 10 independent experiments, 4-6 tumor cell clones and >10 mice per replicate. Numbers within the gates indicate percent of stromal cell subsets.

C) Anti-ESAM staining (red line) on viable (7-AAD$^-$) CD45$^-$ Ter119$^-$ gp38$^-$ CD31$^+$ BECs.

D) Stromal cells from untreated mice were subjected to qRT-PCR analysis (pooled RNA from 5 independent flow cytometry sorting experiments; n=4-5 mice per sort). Gene expression depicted relative to *Gapdh*.

E) Volcano plots show differential expression of genes in lymphoma versus control (fold change, FC log$_2$ >1.5; p≤0.01).

F) Venn plot depicts genes that were selectively upregulated in tumor-exposed vascular stroma cells versus controls (p≤0.001, FC log$_2$ ≥1.5). **G)** A heatmap showing differential gene expression of 114 jointly upregulated genes; changes are indicated by the color scale. In **E-G),** a Student's t-test was applied.

Figure 3. The pro-angiogenic milieu in lymphoma-bearing LNs leads to abnormal vessel density and morphology

A) RT-qPCR array analysis with RNA from total LNs of either control or Eμ-*Myc* lymphoma recipient mice with low and medium tumor burden (n=3 independent

34

experiments, n=10 pooled mice per group). Altered gene expression levels are depicted as x-fold expression ($\log_2$) normalized to control LNs (x-axis, baseline). Bars represent means ± SEM; t-tests were used to test if means are different from 0. *, P≤0.05, **, P≤0.01, ***, P≤0.001.

B) GEP of sorted follicular B cells from controls and Eμ-*Myc* lymphoma cells from transplanted mice (n=3 independent experiments, n=3 different Eμ-*Myc* clones). A representative "Angiogenesis" related GSEA signature (top) and a signature of genes encoding secreted proteins is shown (bottom). Expression changes are depicted according to the color scale.

C) Confocal microscopy analysis of inguinal LN vessels from control and Eμ-*Myc* lymphoma-recipient mice at days 8-12. A dashed line indicates the T cell zone. Representative images are maximum intensity projections of 100 μm z-stacks of anti-CD31 stained sections.

D) Quantification of CD31$^+$ surface area within the paracortical T cell zone (CD3$^+$); 1-2 paracortical T cell zones per LN were analyzed and 3D quantitative analysis of CD31$^+$ surface integrates all z-stacks; n=4-5 mice per condition.

In **D**), bars are mean values; Mann-Whitney U-test.

E, F, H-J) GSEA of microarray data from BECs as displayed in **Fig. 2** were performed.

G), a heat map of genes from a *VEGFC^{156S}/VEGFR3* gene signature in Eμ-*Myc* lymphoma challenged BECs compared to untreated BECs (FC cut off <-0.2 or >0.2). Expression changes of 10 most up- or down-regulated genes are indicated by the color scale.

Figure 4. Angiocrine effects of Eμ-*Myc* lymphoma are characterized by a hypersprouting phenotype

A-C) LN sections (100 μm in z) from control (n=4) or Eμ-*Myc* lymphoma transplanted (n=9) *Cdh5-GFP* reporter mice (tamoxifen induced) were analyzed by confocal microscopy. 3D reconstructions were obtained from z-stacks (4x4 tiles; 63x objective; 540x540x100 μm). Shown are maximum intensity projections and quantitative analysis of GFP$^+$ surface area relates to single fields of view. In **B)**, number of loops and in **C)** number of branching points per 4x4 tiles normalized per vessel length; data points represent distances (μm) between loops and branching points. Bars are mean values; Mann-Whitney U-test, **, P≤0.01. Scale bar, 100 μm.

D) Vascular perfusion of *Cdh5-GFP* reporter mice transplanted with Eμ-*Myc* lymphoma cells (d 9-11 after lymphoma cell injection) was determined by i.v. injecting 100 μg isolectinB4 (IB4). Representative fluorescent images of perfused and non-perfused blood vessels with isolectin (IB4, red) and Cdh5-GFP (green) are presented on the top, quantification of patent loops and capillaries (GFP$^+$/IB4$^+$ vessels relative to total GFP$^+$ vessels) is given below. Bar graphs represent mean values for size-grouped vessels, and numbers in the bars indicate the number of vessels analyzed. n>2 independent experiments, n=5 animals analyzed.

E) Visualization of atypical tip cells, aberrant filopodia and blebs in LN from untreated (middle) and lymphoma-recipient *Cdh5-GFP* reporter mice (right). Representative images from at least n=4 mice per group are shown. Scale bar, 10 μm. In **A-E),** all vascular analysis refers to the T cell zone.

36

F) Anti-ESM1 staining of LN vasculature from lymphoma-recipient *Cdh5-GFP* reporter mice. At least 4 mice were investigated, shown are representative images. Scale bar, 5 μm and 25 μm.

Figure 5. BEC-specific LTβR signaling is crucial for aggressive lymphoma-induced LN angiogenesis

A, B) Eμ-*Myc* and Eμ-*MycxLtα$^{-/-}$* tumor cells were i.v. transferred into Wt recipients (n=3 independent experiments, n>10 mice per group; control, n=10 mice). At day 8-12, an qRT-PCR cell cycle-associated gene array was performed with RNA from BECs. Gene expressions were calculated relative to *Gapdh*, the scatter plot shows all genes with a cutoff $p<0.05$ and a FC>2 ($\log_{10}$) highlighted in red. A Student's t-test was applied.

C) Treatment of Eμ-*Myc* lymphoma-transferred mice with 100 μg LTβR-Ig (n=11) i.p., or with control mouse IgG1 (MOPC21, n=11). Tumor load of LNs was assessed at day 8-12 by flow cytometry. Bars indicates the ratios of tumor cells in controls, set arbitrarily at 1, and LTβR-Ig treated animals. n=5 independent experiments; Wilcoxon signed-rank test.

D) Immunostaining of inguinal LN vessels (CD31$^+$) from MOPC21 and LTβR-Ig treated lymphoma-bearing mice. Scale bar, 500 μm. Representative images are maximum intensity projections of 100 μm z-stacks. Analysis of the vasculature in **D-J)** in the paracortical T cell zone.

E) CD31$^+$ surface expression; n=4 independent experiments, with 5-6 animals per group, and 1-2 T cell zones per section and per LN analyzed. Bars represent mean values; Student's t-test.

37

F) Lymphoma recipient mice were injected with BrdU for 3 days. CD31$^+$ gp38$^-$ BECs were analyzed by flow cytometry for BrdU$^+$ uptake relative to MOPC controls, set arbitrarily to 1 (n=6 independent experiments, with 4-5 mice pooled per group and per condition); Wilcoxon signed-rank test.

G) Eμ-*Myc* lymphoma B cells were transferred into *Cdh5-GFP* mice. Animals were treated as in **C** (LTβR-Ig, n=7; MOPC21, n=6). At day 8-12, LN sections were analyzed.

H, I) Quantitation of vessels based on 3D reconstruction analysis of confocal imaging z-stacks (4x4 tiles, 63x objective; 540x540x100 μm). Shown are maximum intensity projections. Scale bar, 100 μm. Graphs showing endothelial surface areas (GFP$^+$) and number of branching points. n>3 independent experiments.

J) *Cdh5-Cre/ERT2* and tamoxifen-induced *Cdh5-Cre/ERT2 x LtβR$^{fl/fl}$* mice were challenged with lymphoma B cells. Tumor load of LNs was quantified at day 8-12; n=8-9 animals, n=2 independent experiments; (**H-J**), bars represent mean values; Mann-Whitney U-test; **K)** Vascular surface was quantitated as in **E)**. Bars represent mean values; Student's t-test.

Figure 6. Lymphoma-induced angiogenesis is governed by the VEGF-C/VEGFR-3 signaling axis

A) Eμ-*Myc* B cells were i.v. transferred into Wt recipients. Animals were administered with anti-VEGFR-2 antibody or with an isotype control antibody at a dosage of 100 μg i.p. At day 8-11, lymphoma cells in LNs were quantified by flow cytometry. Data points represent the ratios of tumor cells among all CD45$^+$ cells (in percent) in isotpye treated mice versus anti-VEGFR-2 treated animals.; n=2 independent experiments.

38

B, C) CD31$^+$ vascular surface areas and branching points in T cell zones from inguinal LNs taken from animals treated with an isotype or an anti-VEGFR-2 antibody. Quantification was done on 3D-reconstructed images as in **Fig. 3C**. Bars represent mean values; in **B, C**), a Mann-Whitney U-test was used.; n.s., non significant.

D) LN from control (n=3-5) and lymphoma exposed mice (n=3-5) were dissected and stroma cell subsets were isolated. Macrophages (CD11b$^+$F4/80$^+$), T cells (CD3$^+$), normal B cells (B220$^+$), and Eμ-*Myc* lymphoma cells (B220$^+$FSC-A^{high} tumor) were also sorted and subjected to RT-qPCR analysis. Error bars indicate mean $\pm$ SEM; n=3-5 independent experiments were performed; Student's t-test.

E) Sera from animals treated with (n=8) or without Eμ-*Myc* lymphoma cells (n=8) were analyzed by a VEGF-C specific ELISA. Data points depict the calculated amount of VEGF-C relative to total protein amounts in 1 ml serum. Bars indicate mean values; n=3 independent experiments; Student's t-test.

F) Sprouting of HUVECS performed in spheroid cultures. Cells were grown in basal growth medium alone (control), or with supplements; additionally, a combination of these factors was used for a 24 h culture. N=40-55 spheroids counted per treatment condition; data points indicate mean values per experiment, n=5-8 experiments were performed; Student's t-test.

G) HUVEC growth factors and LTα1β2 (LT) were added to basal growth medium (control) for 6 h. VEGFR-3 surface density was analyzed by flow cytometry and expressed as geo mean fluorescence intensity; in **G)**, n= 8 independent experiments; Student's t-test.

H) LN and spleen protein lysates were generated from control (n=6-7) and Eμ-*Myc* lymphoma transferred mice (n=6-7). VEGF-C was detected in immunoblot, anti-GAPDH was used as a loading control. Images were cropped for presentation and displayed bands are representative of all samples.

I) The ratios of the different trimming forms of VEGF-C relative to GAPDH are presented as bar graphs; n> 3 independent experiments, with n=3 different tumor cell clones. Bars represent mean values.

J) Gene expression of *Ccbe1* as determined by qRT-PCR. FRCs, BECs, LECs and normal B cells from control mice (n=3-5) were sorted, or cells were recovered from *Eμ-Myc* lymphoma transplanted mice (n=3-6); n>3 independent experiments.

K) *Vegfr3* gene expression; control (n=3-5), Eμ-*Myc* lymphoma transplanted mice (n=3-5); at least 3 independent experiments. Error bars indicate mean ± SEM; **I-K)** a Mann-Whitney U-test was applied.

L) *Vegfr3-GFP* reporter mice challenged with Eμ-*Myc* lymphoma cells (n=3 mice) for 8-12 days. FRCs, BECs and LECs were differentiated by anti-CD31 and anti-gp38 staining. Shown are representative histograms of VEGFR-3 (GFP$^+$) expressing cell subsets. On the right, VEGFR-3 expression in vascular subsets from control and *Eμ-Myc* lymphoma bearing mice assessed by immunostaining and flow cytometry analysis. Error bars for mean fluorescence values indicate mean ± SEM.; n= 3 mice/group.

M) Wt mice received a total of 2-4 x10^5 Eμ-*Myc* tumor B cells i.v. At day 1-7, animals were administered with SAR131675 (n=4 mice) or with carrier solution (n=6) p.o. At day 8-9, lymphoma cells in LNs were quantified by flow cytometry relative to all leukocytes. Bars (mean values) represent the ratios of control and SAR131675 treated animals. On

40

the right, $CD31^+$ vascular surface areas in inguinal LNs from these animals were analyzed by confocal microscopy;, n=3 independent experiments.

N) Wt mice were inoculated s.c. with MCA313 fibrosarcoma cells. Upon palpable tumor growth, animals were treated with SAR131675 or with carrier solution p.o. for up to 16 d. Tumor weight of resected tumors was measured after sacrificing the animals; **M, N)**, a Mann-Whitney U-test was applied; n.s., non significant.

Figure 1

Figure 2

Figure 3

Figure 4

Figure 5

A unique angiogenic milieu exists in lymph nodes whereby VEGFR-3 and LTβ receptor take the lead in lymphoma angiogenesis when VEGF-A availability is disturbed.
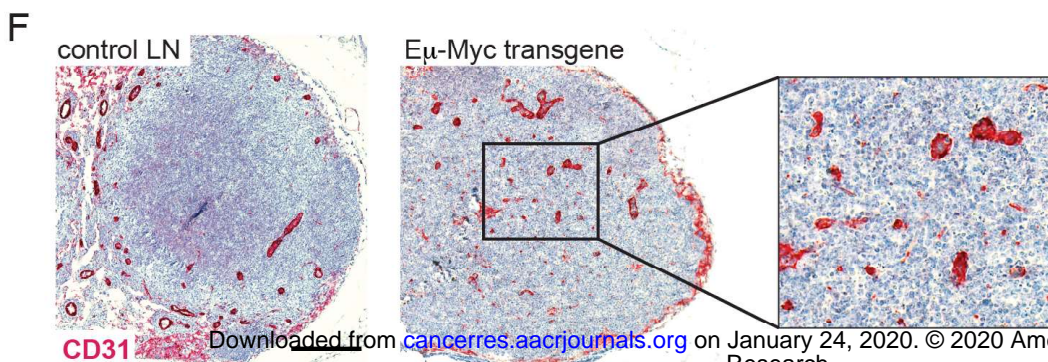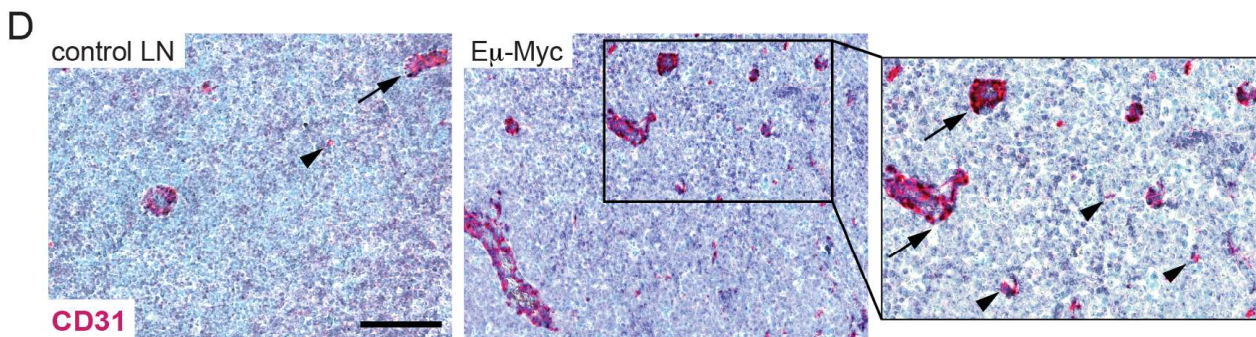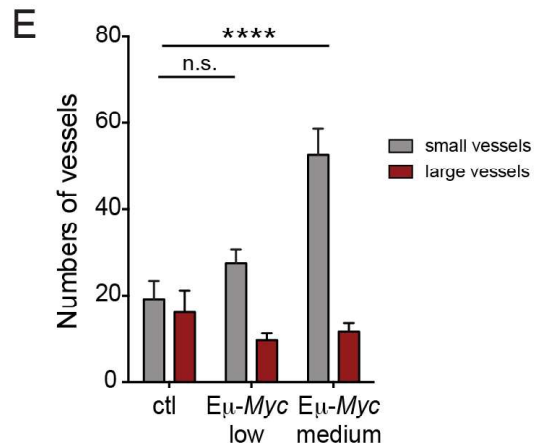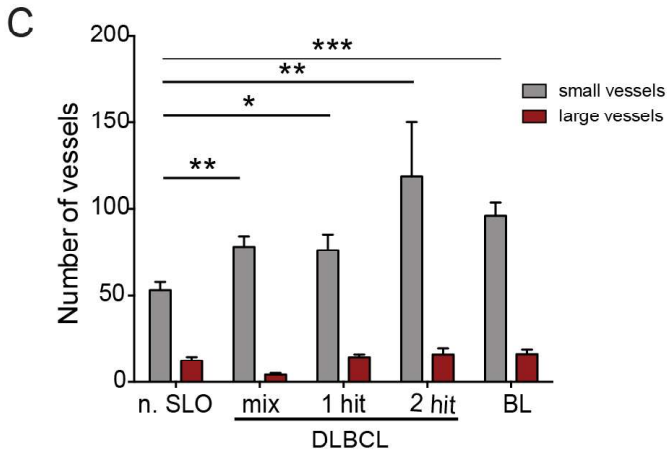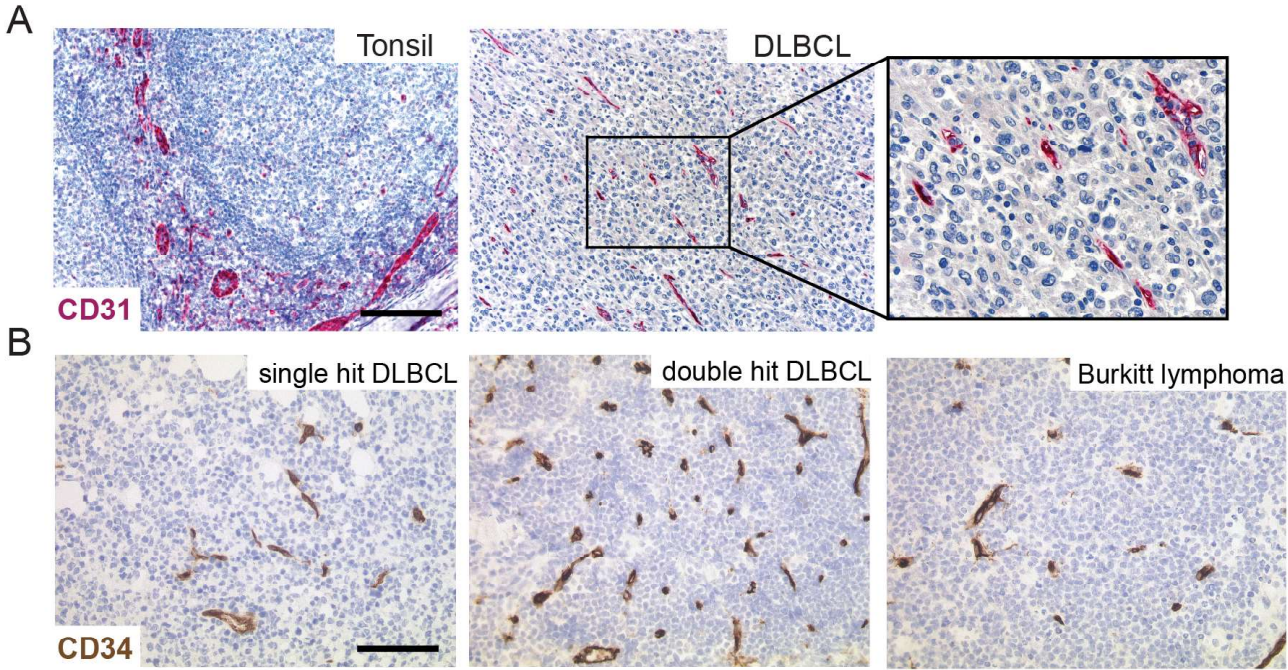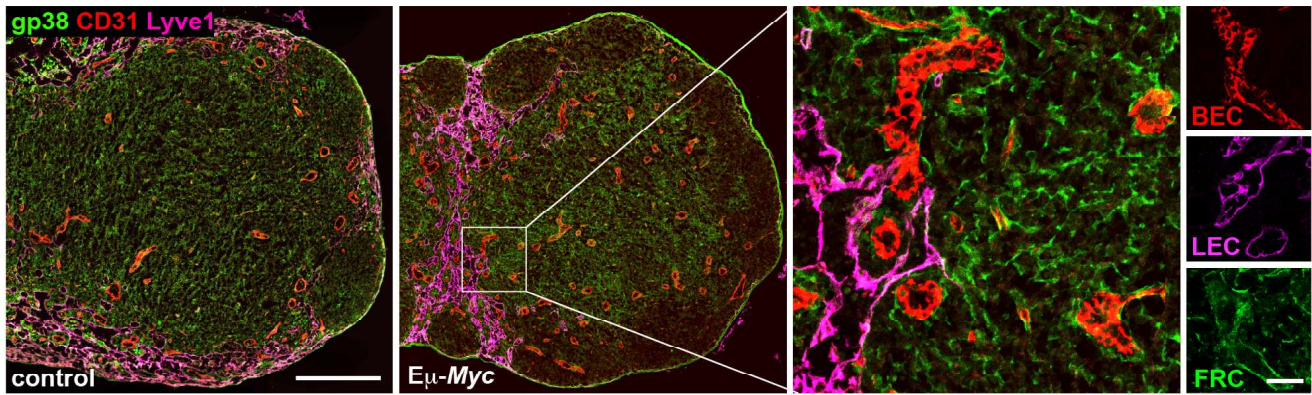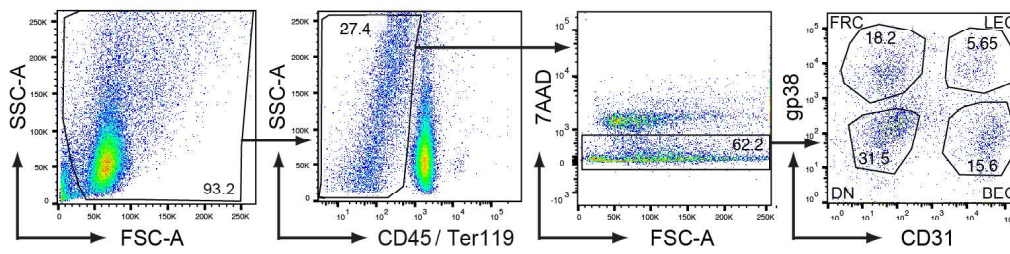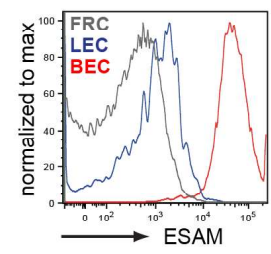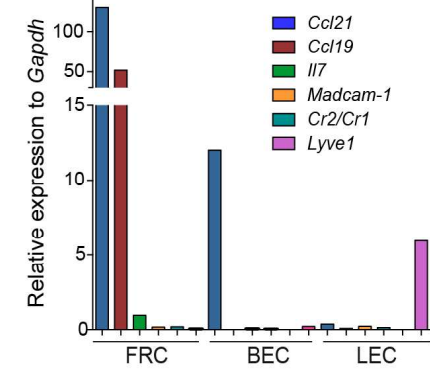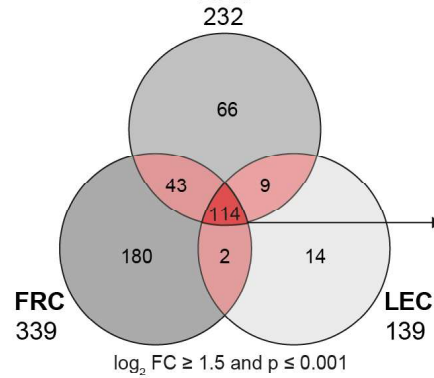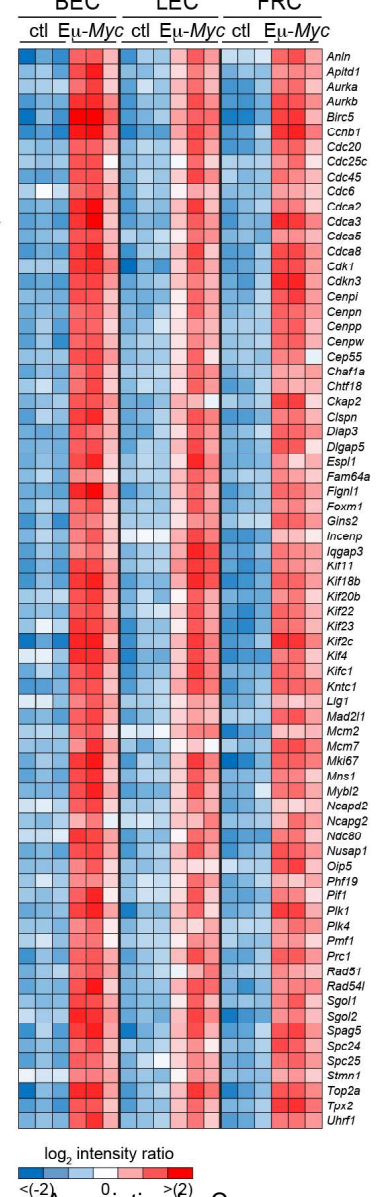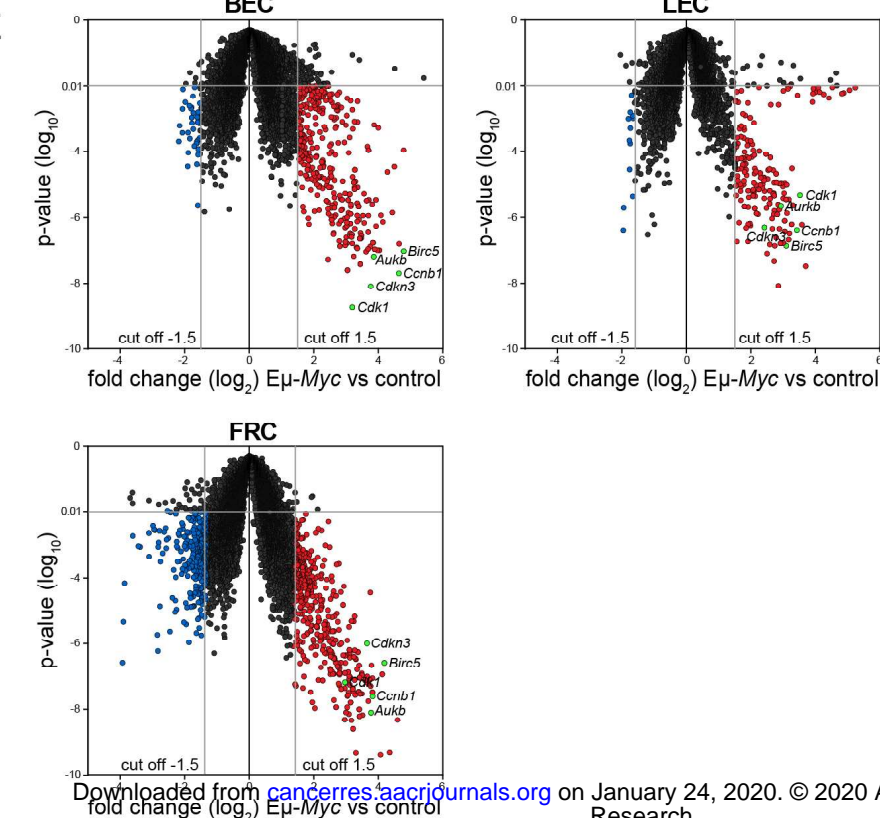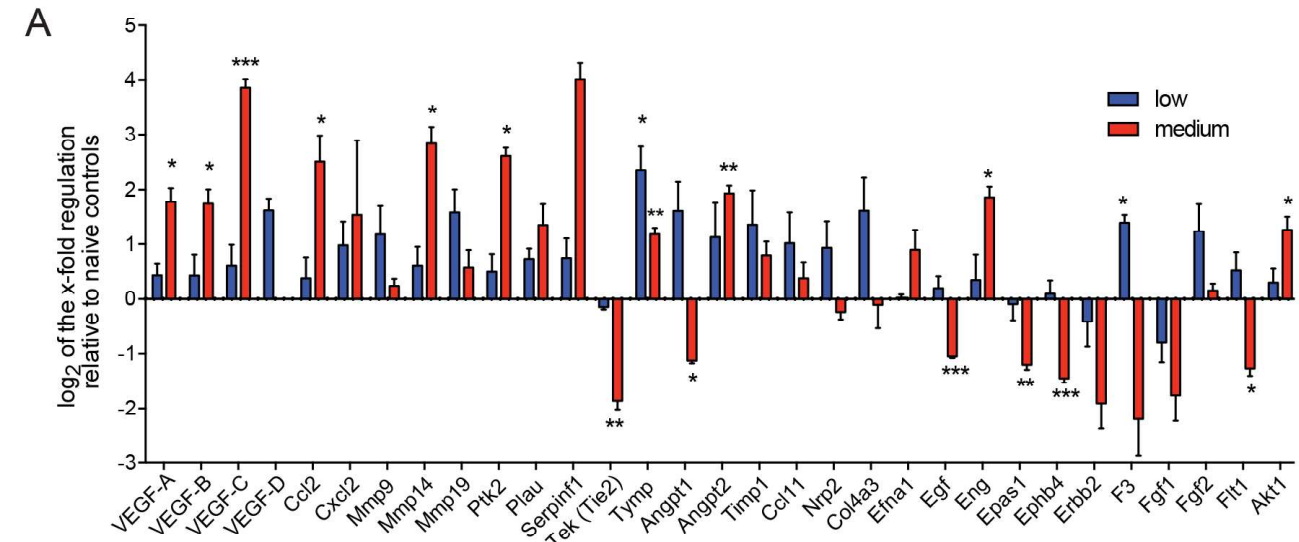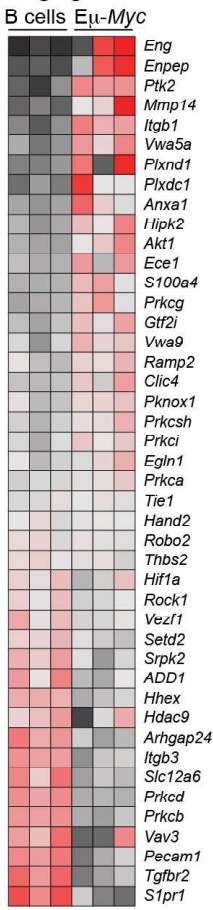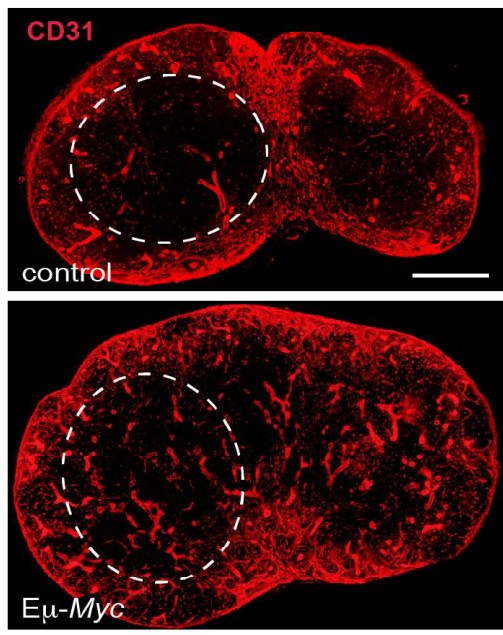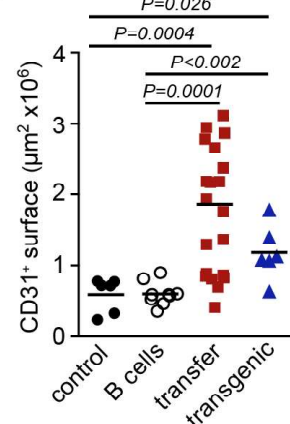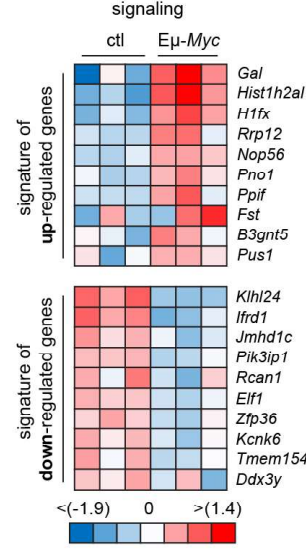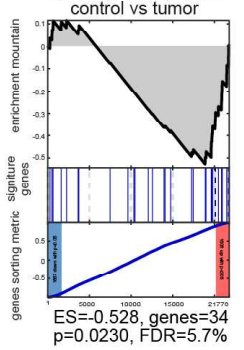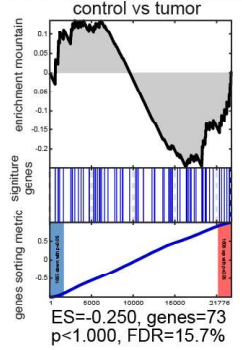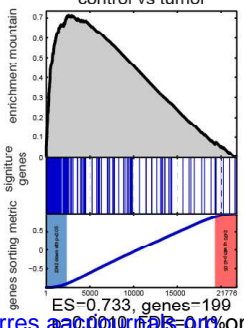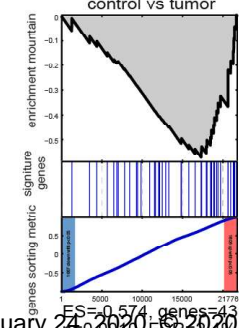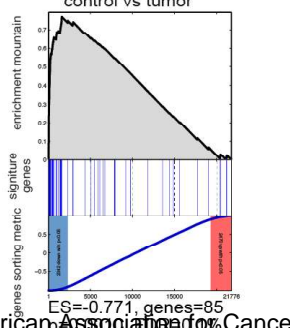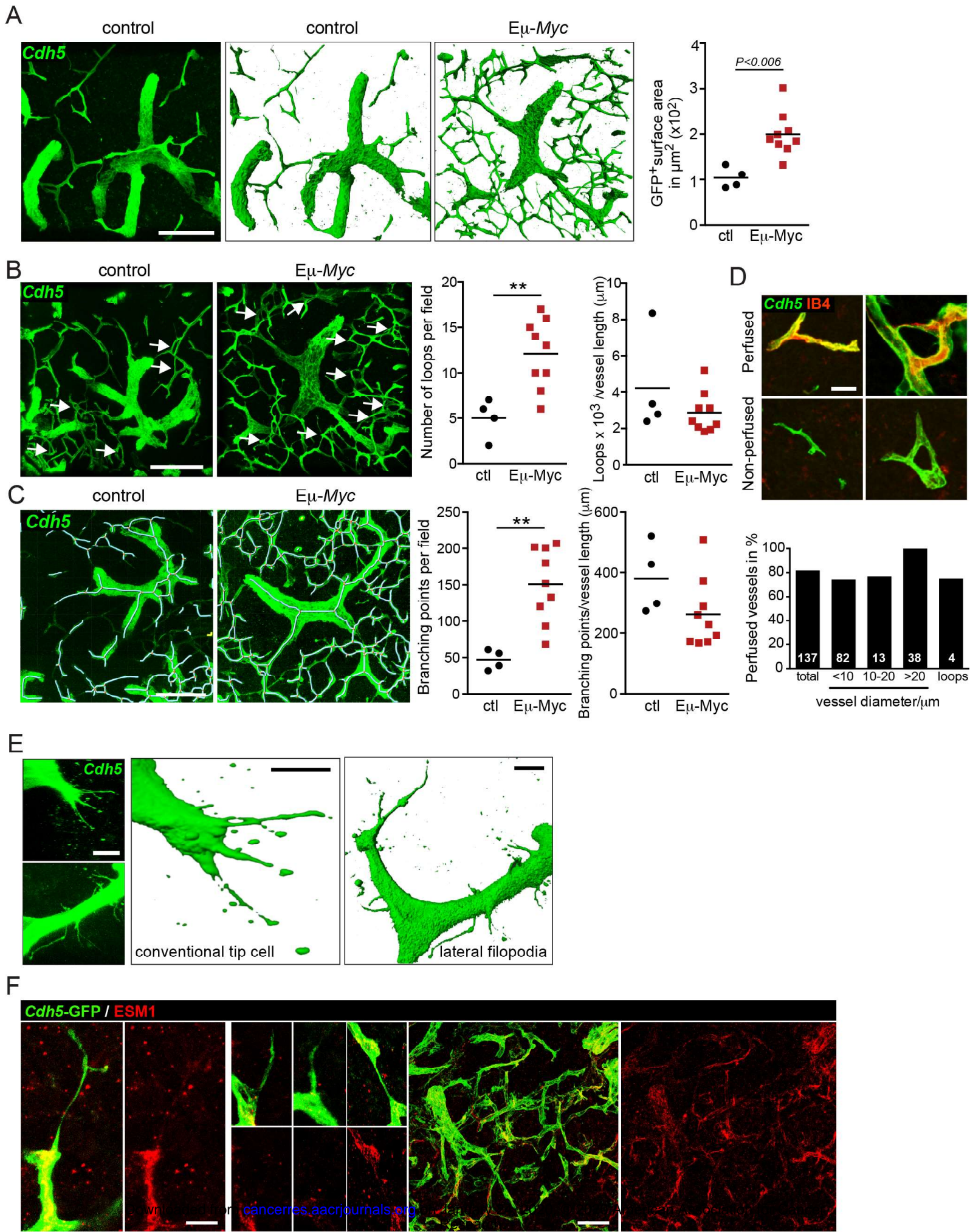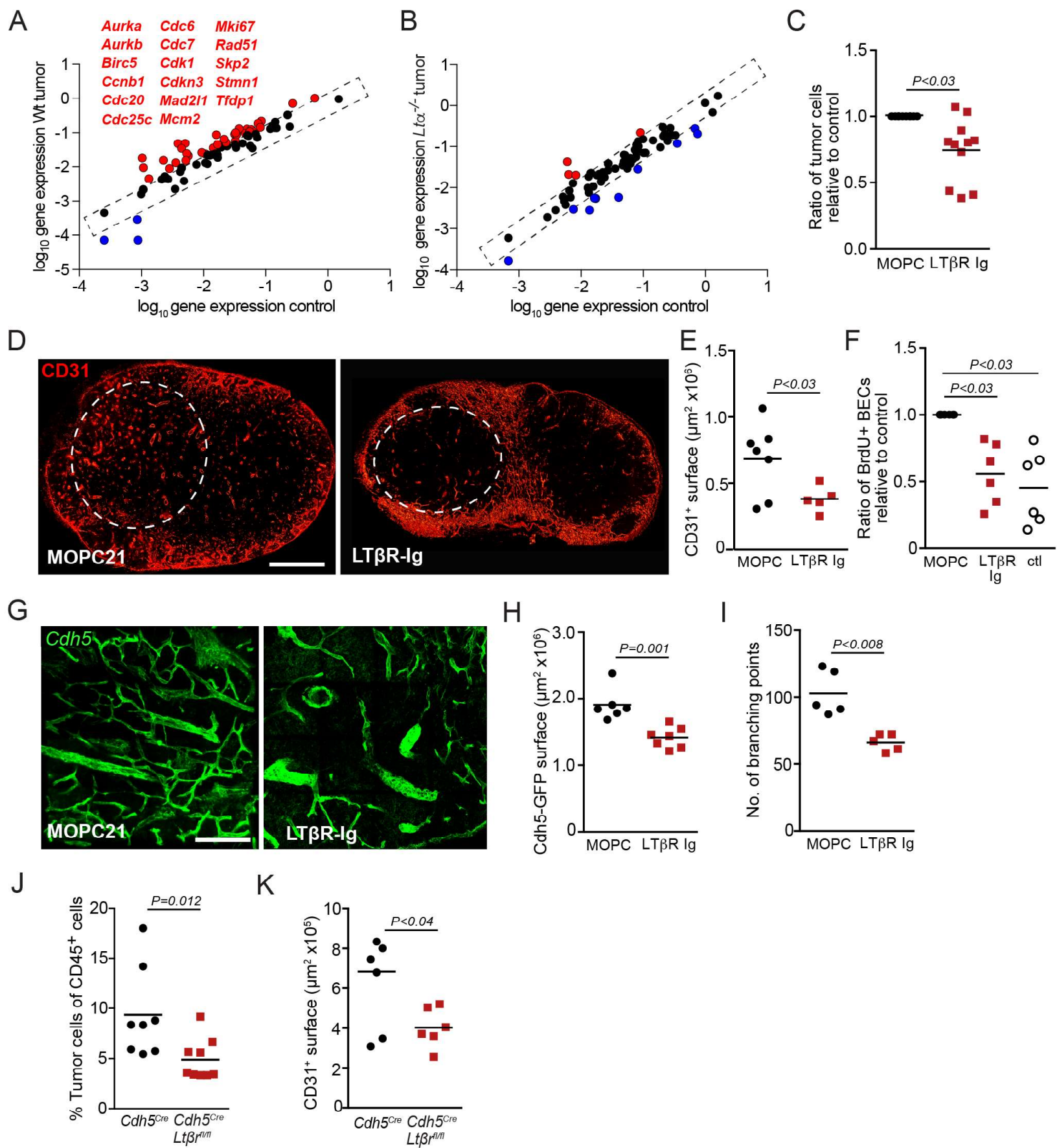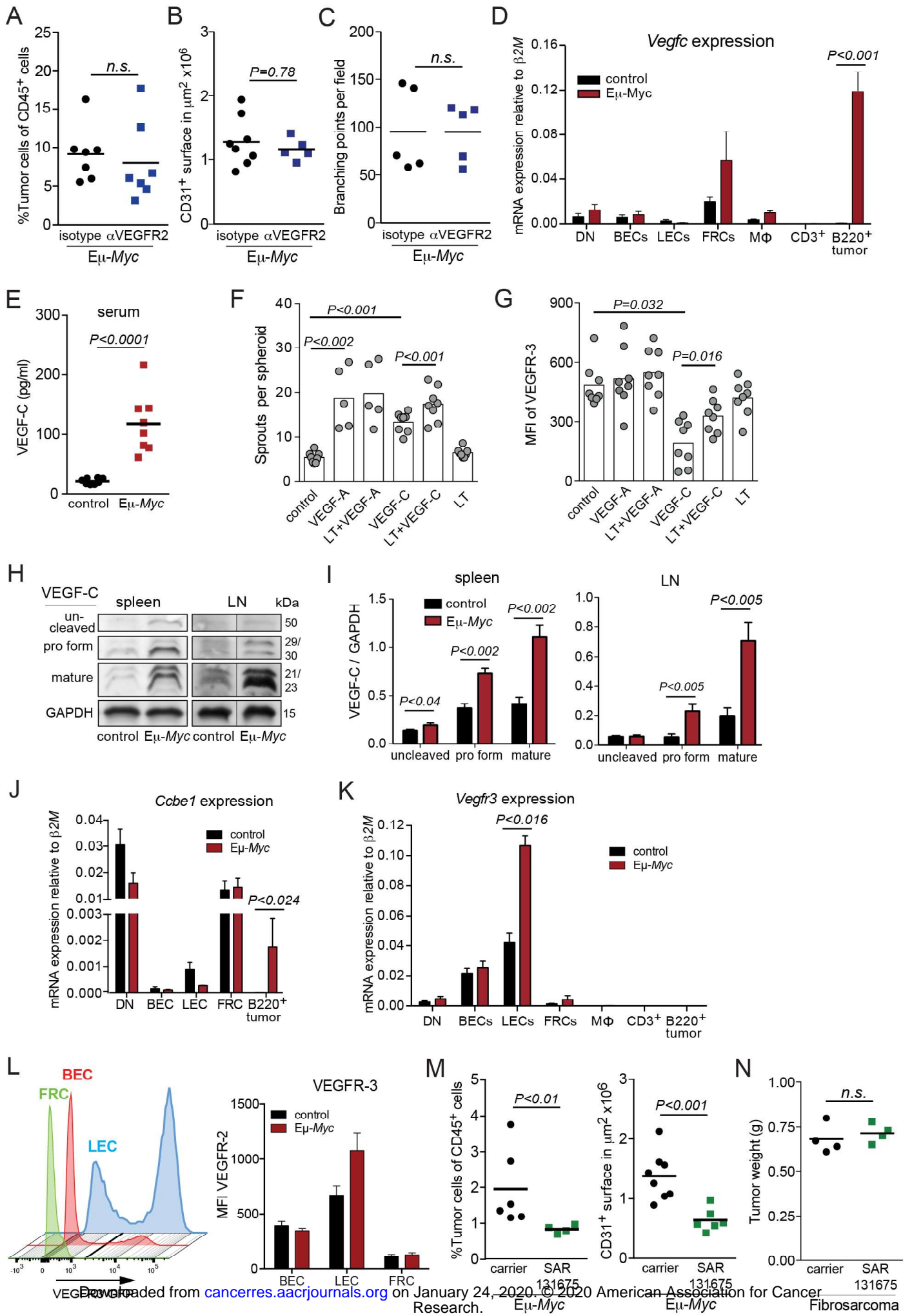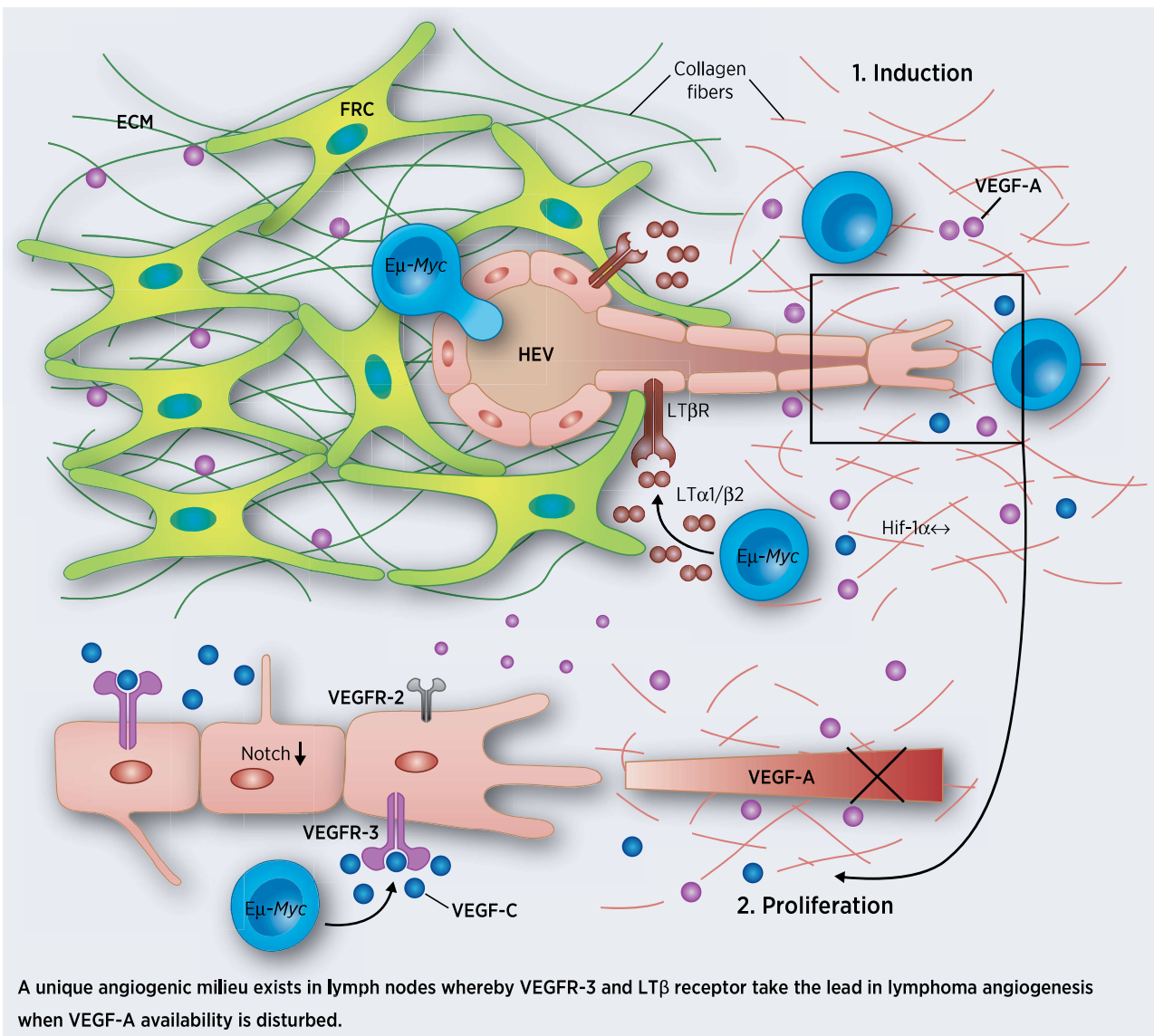
Cancer Research

The Journal of Cancer Research (1916–1930) | The American Journal of Cancer (1931–1940)

AACR American Association for Cancer Research

Lymphoma angiogenesis is orchestrated by noncanonical signaling pathways

Marleen Gloger, Lutz Menzel, Michael Grau, et al.

Cancer Res Published OnlineFirst January 13, 2020.

Updated version	Access the most recent version of this article at: doi:10.1158/0008-5472.CAN-19-1493
Supplementary Material	Access the most recent supplemental material at: http://cancerres.aacrjournals.org/content/suppl/2020/01/13/0008-5472.CAN-19-1493.DC1
Author Manuscript	Author manuscripts have been peer reviewed and accepted for publication but have not yet been edited.

E-mail alerts	Sign up to receive free email-alerts related to this article or journal.
Reprints and Subscriptions	To order reprints of this article or to subscribe to the journal, contact the AACR Publications Department at pubs@aacr.org.
Permissions	To request permission to re-use all or part of this article, use this link http://cancerres.aacrjournals.org/content/early/2020/01/13/0008-5472.CAN-19-1493. Click on "Request Permissions" which will take you to the Copyright Clearance Center's (CCC) Rightslink site.